Observation and explanation of one-dimensional x-ray speckle patterns from synthetic multilayers

I. K. Robinson
University of Illinois, Urbana, Illinois 61801

R. Pindak and R. M. Fleming
AT&T Bell Laboratories, Murray Hill, New Jersey 07974

S. B. Dierker
University of Michigan, Ann Arbor, Michigan 48109

K. Ploog
Paul-Drude-Institüt für Festkörperelektronik, D-10117 Berlin, Germany

G. Grübel, D. L. Abernathy, and J. Als-Nielsen
European Synchrotron Radiation Facility, 38043 Grenoble, France
(Received 15 March 1995)

Using the new "Troika" x-ray undulator beamline at the European Synchrotron Radiation Facility, we have succeeded in measuring coherent diffraction ("speckle") patterns from artificial multilayers. The patterns are unusual in that they are unremarkable in the scan direction perpendicular to the Bragg angle, showing a single peak of the width of the Fraunhofer maximum, but have dramatic structure in the direction of the Bragg angle. This is shown to be consistent with the extreme asymmetry of the geometry that causes more than one well-ordered domain of the sample to fall within the coherently illuminated region. The patterns are sufficiently simple that we are able to model them reasonably well by fitting explicit phase parameters to a fixed number of illuminated "blocks." Two fitting procedures are described that may have some general utility.

I. INTRODUCTION

New, brighter, undulator sources of x rays offer considerable possibilities for altogether different kinds of diffraction experiments. One of these possibilities is to utilize the improved coherence of the beam, which is a quantity associated directly with the source brightness. If a diffraction experiment is carried out with an x-ray beam that is largely coherent, the observed intensity will depend on the relative *phases* of the scattering of all component parts of the illuminated sample, in addition to all the usual atomic-level structural contributions. In a sample made up of a mosaic of domains, the phases are related to the relative *positions* of the domains. Much of the excitement in the nascent coherent diffraction ("speckle") field[1] stems from the possibility one day of achieving atomic-resolution fluctuation spectroscopy: in the case of a sample whose internal domain structure is due to intrinsic fluctuations, such as those associated with a phase transition, the *time dependence* of the fluctuation may therefore be probed by monitoring the variations in *intensity* of the coherent diffraction signal.

Here we investigate the practicality of interpreting the coherent diffraction from a simple structure, an artificial multilayer prepared by molecular beam epitaxy (MBE). We first describe our measurements, which were made during an experimental run that utilized undulator radiation for coherent diffraction, at the European Synchrotron Radiation Facility (ESRF) in Grenoble. Then we describe our attempts to understand the data at a quantitative level, by constructing a "random-phase model" in which the illuminated part of the sample is considered to be a "phase structure" made up of discrete scattering "blocks," each with its own phase relative to its neighbors.

Coherent diffraction of x rays is a relatively new subject, with relatively little published work to date. One significant previous study[2] investigated the grain structure induced in a sample of Cu_3Au by quenching from above its disordering temperature. In other static work, speckle has been recorded from a structured polymer thin film.[3] Recently, experimental time-correlation functions have been observed in two systems, Fe_3Al near to its critical temperature,[4] and in small-angle scattering from colloidal gold.[5] Historically, temporal effects have been discussed mainly in the context of coherent light scattering, where the time structure of a scattered signal can be readily interpreted in terms of diffusion or motions of scattering objects.[6] The information so obtained is always on a length scale of the wavelength of light, and so the traditional technique is inherently unable to probe contrast on an atomic scale. X rays offer the appealing possibility of extending these powerful techniques to probe motions on the scale of individual atoms.

0163-1829/95/52(14)/9917(8)/$06.00

I. EXPERIMENTAL CONFIGURATION

The measurements were made at the ID10 "Troika" beamline[7] at ESRF in which the radiation source is a permanent magnet undulator. The beam was monochromated with a single-bounce sideways-scattering water-cooled thin Si(220) crystal located 45 m from the source and set to an energy of 12 keV ($\lambda=1.05$ Å). The thin crystal passed a significant fraction of the power of the beam to assist the cooling.[8] The total incident power was reduced further by closing horizontal slits at the 27 m point of the beamline. Harmonics in the diffracted beam from the monochromator were filtered by reflection from a SiC mirror which restored the beam to the horizontal plane. The sample was located at 46 m, mounted on a four-circle diffractometer, oriented with its principal axis vertical.

The most critical parameter in a coherent diffraction experiment is the lateral (or transverse) coherence length. A perfectly monochromatic plane wave has a constant phase everywhere in a plane perpendicular to its wave vector **k**. Two monochromatic plane waves propagating in directions differing by an angle $\Delta\theta$ will have a phase difference of 2π within this plane at a distance $\zeta_\perp$, the lateral coherence length, given by $(k\Delta\theta)\zeta_\perp=2\pi$. $\Delta\theta$ is determined by the finite size of the x-ray source, which either is intrinsic to the storage ring or may be set by a slit or pinhole inserted into the beam. If a source of size w is located at a distance W from the point of observation, then $\Delta\theta=w/W$, and $\zeta_\perp=(2\pi/k)\Delta\theta=W/w$. The intrinsic undulator source width at ID10 is not isotropic, but has $w_H=1026$ μm [full width at half maximum (FWHM)] in the horizontal and $w_V=225$ μm (FWHM) is the vertical directions. We therefore made use of the horizontal slit at $W_1=19$ m, set to an opening of $w_1=100$ μm, to satisfy $W_1/w_1\approx W/w_V$, to obtain an approximately isotropic lateral coherence length of $\zeta_\perp=21$ μm at the sample position, $W=46$ m.

The longitudinal coherence length $\zeta_\parallel$ is determined solely by the bandwith of the monochromator, $\zeta_\parallel=\lambda/(\Delta E/E)$. For symmetric Si(220) at 12 keV, $\Delta E/E$ is estimated to be 5.1×10^{-5}, giving $\zeta_\parallel=2$ μm. The longitudinal coherence must be longer than the maximum path-length difference (PLD) in the experiment, in order to observe coherence effects. In our experiment, which uses the symmetrical extended-face geometry, the PLD is $\mu^{-1}\sin^2\theta_B$, where μ^{-1} is the absorption length and θ_B is the Bragg angle of diffraction. μ^{-1} is estimated to be 28.7 μm and $\theta_B\approx0.79°$ for the sample and measurements we will be referring to, giving a PLD of only 0.006 μm. From this we conclude that the longitudinal coherence is sufficiently good that it can be ignored.

To select a coherent beam for the experiment, it is necessary to place an aperture in front of the sample with an opening smaller than $\zeta_\perp=21$ μm. We used a nominal $d_1=7$ μm circular aperture ("pinhole") laser drilled into a 50 μm Pt sheet, centered behind a 0.5 mm hole drilled in a 1 mm thick Ta plate. This pinhole was mounted on a precision X-Y stage with submicrometer repeatability. A nominal $d_1=3.5$ μm front pinhole was also used for calibration. This front pinhole was located approximately

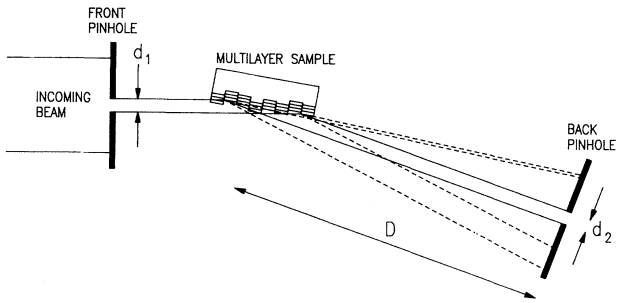

FIG. 1. Layout of the experiment. The front pinhole selects a sufficiently small beam from the monochromatic undulator beam that it is essentially phase coherent across its size d_1. This illuminates the multilayer sample at the Bragg angle for one of the superlattice reflections perpendicular to its surface. The microscopic "block" structure assumed in our data analysis is drawn exaggerated for clarity. The scintillation x-ray detector is located behind the back pinhole which is a sufficient distance D from the sample that it measures essentially the angular distribution of the scattering. In the settings corresponding to the data of Figs. 3 and 4, $d_1=7$ μm, $D=1.3$ m, and $d_2=20$ μm.

100 mm before the sample, at the center of the four-circle goniometer. A second, back pinhole of diameter $d_2=20$ or 5 μm was installed on the 2θ arm of the diffractometer at a distance $D=1.3$ m from the sample, and followed by a scintillator/photomultiplier detector. The motion of the diffractometer and pinholes was coordinated by the beamline experimental computer. The experimental layout is sketched in Fig. 1. The MBE-grown sample consisted of 377 repetitions of alternating layers of GaAs and AlAs on a GaAs(100) substrate. The period was 13.5 layers or 38 Å.

II. RESULTS

The coherence of a beam is usually measured as its fringe visibility or contrast.[9] In order to observe this, scans were made of the direct beam without a sample. The results are shown in Fig. 2, for the smallest pinhole diameters $d_1=3.5$ μm and $d_2=5$ μm, in order to obtain the maximum visibility. The Fraunhofer diffraction of the front pinhole is clearly seen in the two perpendicular scans of the back pinhole. The data are presented as counting rate vs back-pinhole position y. We distinguish the direction parallel to the motion of the diffractometer's 2θ arm as $y_\parallel$ (horizontal in our setup) from the perpendicular direction as $y_\perp$ (vertical in our setup). Many fringes are seen with slightly different contrast in the four directions examined; this is believed to be a property of the precise shape of the pinhole, and the straightness of its edges. The scan marked (a) in Fig. 3 is Fraunhofer diffraction obtained with a $d_1=7$ μm, $d_2=5$ μm setting. The fringes in Fig. 3(a) are also seen to fade away and then resume as a function of the off-axis distance; this is also due to a deviation from roundness of the 7 μm front pinhole, which appears to be worse than the $d_1=3.5$ μm pinhole used in Fig. 2.

The sample was then installed and aligned on the first-order diffraction of the superlattice. Following the usual

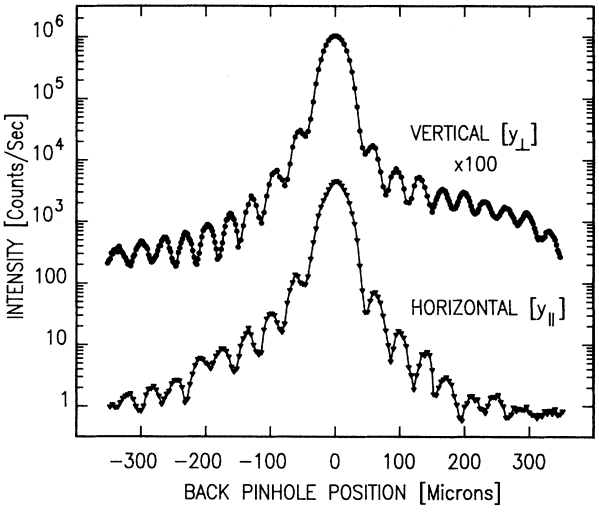

FIG. 2. Fraunhofer diffraction measured for the direct x-ray beam without a sample. A $d_1=3.5$ μm front pinhole and $d_2=5$ μm back pinhole were used to ensure good visibility of the fringes. Scans of the back pinhole were made along two perpendicular directions, as indicated.

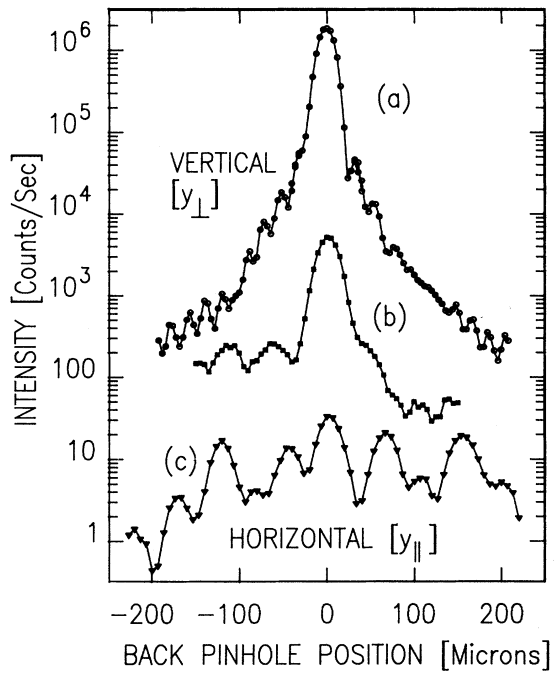

FIG. 3. (a) Measurement of the Fraunhofer diffraction from a $d_1=7$ μm front pinhole resolved by scanning a $d_2=5$ μm pinhole in front of the detector along the vertical direction. The visibility of the fringes is considerably reduced from those from Fig. 1. (b) Coherent diffraction of the $(000)^+$ peak from the multilayer sample along the same direction. 7 μm front and 20 μm back pinholes were used. The central peak has the same width as the Fraunhofer diffraction in (a). (c) Coherent diffraction of the same peak along the *horizontal* direction. The same 7 μm front and 20 μm back pinholes were used. Several peaks are observed, with each peak having the same width as the Fraunhofer diffraction in (a).

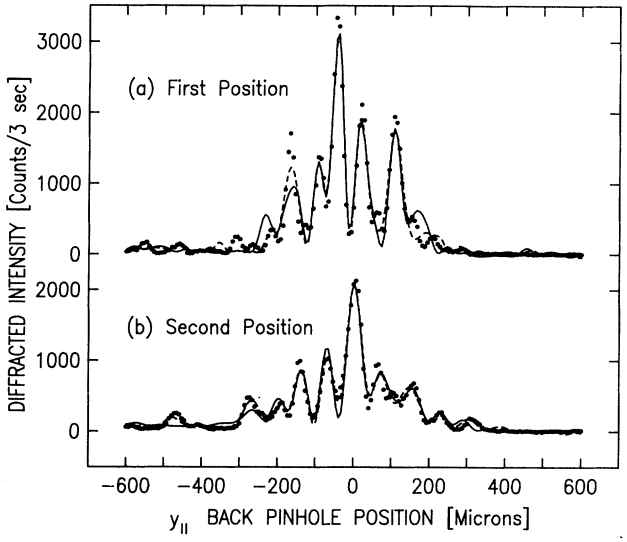

FIG. 4. Intensity distribution of the speckle patterns recorded for the $(000)^+$ superlattice peak of he 38 Å period GaAs/AlAs multilayer, as a function of the back pinhole position $y_\parallel$, measured parallel to the scattering plane along the direction of the Bragg angle The two sets of data (a) and (b) correspond to two different positions on the sample, separated by 20 μm in *lateral* position (perpendicular to the page in Fig. 1). The full curve is the best fit to Eq. (1) using the phase structure of line (a) in Fig. 6 below; the dashed curve shows the improvement when the block sizes are also allowed to vary, corresponding to the phase structure of line (b) of Fig. 6.

convention, this peak is a satellite of the origin of reciprocal space, so is denoted $(000)^+$. The diffraction coming from the sample was analyzed again in the two directions $y_\perp$ and $y_\parallel$, and is shown in Figs. 3(b) and 3(c), respectively. The $y_\perp$ scan shows a single peak 20 times more intense than the background features, with the same width as the direct beam in Fig. 3(a). The $y_\parallel$ scan shown in Fig. 3(c) is totally different, and shows many peaks within a broad envelope function. The individual peaks each have approximately the 55 μm minimum-to-minimum width of the corresponding scan across the direct beam in Fig. 3(a), which has about the width expected for the circular Fraunhofer diffraction from the nominally round $d_1=7$ μm source pinhole itself, $1.22\times 2\lambda D/d_1=51$ μm, minimum to minimum.[9]

The distribution of peaks in Fig. 3(c) is the "speckle" pattern, and its interpretation is the main focus of this paper. An experimental verification that this depends sensitively on the fine structure of the sample is shown in Fig. 4. The only difference between curves (a) and (b) in Fig. 4 is that the front and back pinholes were shifted perpendicular to the scattering plane by 20 μm in the $y_\perp$ direction (out of the plane of the page in Fig. 1) to illuminate a fresh part of the sample. Although its qualitative features (e.g., overall width) are preserved, the heights and positions of all the peaks are substantially changed between the two patterns.

III. GENERAL OBSERVATIONS

The dramatic difference between scans (b) and (c) of Fig. 3 shows that the speckle pattern is one dimensional with significant speckle features in the $2\theta(y_{\parallel})$ direction only. At first glance this result is enigmatic, since there is nothing anisotropic about the fabrication of the sample, which should be cylindrically symmetric. In conventional diffraction experiments, a peak that is broadened in the 2θ direction is interpreted as due to variations of lattice parameter, just as the perpendicular directions correspond to mosaic spread. It is of course perfectly reasonable that an artificial multilayer sample should have intrinsic *d-spacing disorder,* but we will show that this is irrelevant to the interpretation of the speckle, except to the extent that it changes the ultimate position of the outermost layers.

We note that the Bragg angle of the $(000)^+$ superlattice reflection, θ_B, is only 0.79°. This grazing angle of incidence onto the multilayer has two important consequences. Since the absorption length of 12 keV x rays in $Ga_{1-x}Al_xAs$ is $\mu^{-1}\approx 28.7$ μm, the penetration depth of the beam into the sample at this angle is $\frac{1}{2}\mu^{-1}\sin\theta_B$, or only 0.20 μm, considerably smaller than the width of the coherent beam emerging from the front pinhole ($d_1=7$ μm). The coherent diffraction effects observed in Fig. 3(c) therefore cannot come from variations of phase of scatterers *along the depth direction.* Instead, since the shape of the illuminated spot on the sample is $d_1/\sin\theta_B=500$ μm in the horizontal and $d_1=7$ μm in the vertical, we conclude that the necessary interference must arise from scatterers spread out *in the lateral directions* instead. The grossly elongated "footprint" explains the apparent anisotropy between $y_{\parallel}$ and $y_{\perp}$.

Comparing Figs. 3(a), 3(b), and 3(c), we see that the size of each speckle peak is the same as the Fraunhofer central maximum. This is a necessary consequence of the fact that a small region of sample is illuminated, and all diffraction is broadened by that finite size. The envelope of all the peaks is considerably broader, however, and this must be (inversely) related to the finite size of each coherently scattering *grain* in the sample, instead. For this reason, we can see that there is a general relationship between the total number of speckle peaks (here about eight) and the number of grains in the sample. This number roughly corresponds to the number of phases of intefering wave needed to construct the speckle pattern as an interference sum. The effective grain size is hence of order 500 μm divided by 8 = 63 μm. This lateral grain dimension is therefore larger than the beam in the transverse direction, and so explains why no substantial speckle was seen in the $y_{\perp}$ direction.

This interpretation is clarified by the corresponding reciprocal-space view of Fig. 5. The $N\sim 8$ independently diffracting "grains" of lateral dimension $w\sim 63$ μm and effective thickness (penetration limited) $t\sim 0.2$ μm are shaded in the real-space picture in Fig. 5(a). These give rise to diffraction peaks in reciprocal space which are strongly elongated along the direction perpendicular to the plane of the sample, q_z. When the coherent-diffraction contributions from each of the N grains interfere together, the speckles that are generated are N times narrower still in $q_{\parallel}$, and give rise to the striped appearance of the spot in Fig. 5(b). A scan of the back pinhole along $y_{\parallel}$ is a conventional 2θ scan, which follows the curved trajectory shown in Fig. 5, cutting across the speckles obliquely. The typical spacing between the speckles can be seen to depend on the Bragg angle via

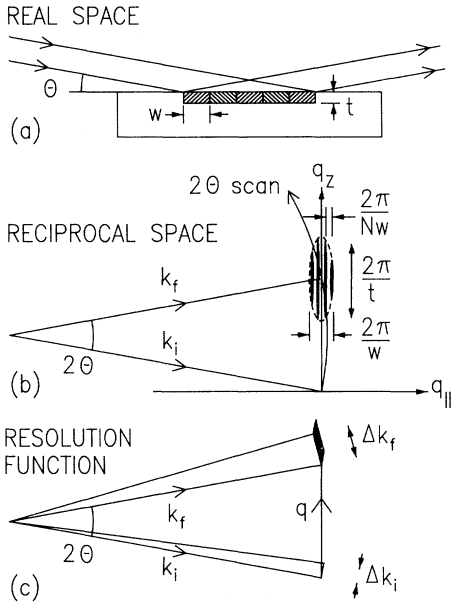

FIG. 5. (a) Real- and (b) reciprocal-space views of the origin of the speckle pattern. The aspect ratio of the elliptical-shaped peak has been grossly underestimated for clarity. The diffraction pattern is sharp and featureless in the direction out of the plane of the page. Further explanation is in the text. (c) Construction of the resolution function. The divergences of the incident and exit k vectors, denoted Δk_i and Δk_f, are determined by the pinholes.

$$\Delta 2\theta_{\parallel}=\frac{\Delta y_{\parallel}}{D}=\frac{2\pi}{Nw}\frac{1}{k\sin\theta_B}\simeq\frac{\lambda}{Nw\sin\theta_B}\ .$$

However, from Fig. 5(a), it is clear that $Nw\sin\theta_B=d_1$, the size of the incoming beam, due to the foreshortening effect. It follows that $\Delta y_{\parallel}=\lambda D/d_1$, which is just the spacing of the side fringes in a normal one-dimensional (1D) Fraunhofer pattern.

Figure 5 also helps to show that d-spacing disorder cannot explain the speckle. Such disorder would modify the distribution of the diffraction peak only along the q_Z direction. Even though this is close to the 2θ direction, the $>1000{:}1$ aspect ratio of each speckle peak ensures that changes along q_z do not alter noticeably the appearance of the oblique scan, which is the speckle pattern. Indeed, conventional diffraction (rotating-anode) measurements of the $(000)^+$ peak of the same sample showed widths in 2θ that were considerably broader than those in Fig. 4, and which correspond roughly to the penetration depth of the sample instead. Another way to see that the 2θ scan resolves the speckles is to construct the resolution function, as in Fig. 5(c). Δk_i $[(2\pi/\lambda)\times(100\ \mu\text{m})(19$

m)$\approx 3\times 10^{-5}$ Å^{-1} FWHM] and $\Delta k_f[(2\pi/\lambda)\times(20\ \mu\text{m})(1.3\ \text{m})\approx 9\times 10^{-5}$ Å^{-1} FWHM] are the incident-beam and diffracted-beam divergences, determined by the beamline apertures and pinholes. While these are already small, they combine at an angle of 2θ as shown to produce a needlelike resolution function with a width of only 1×10^{-6} Å^{-1} in the direction that matches the speckles, sufficient to resolve their spacing of 1.3×10^{-6} Å^{-1}.

IV. RANDOM-PHASE MODEL

For reasons stated above, the phase variations necessary to produce the observed speckle must therefore be due to *lateral* variations of scattering phase. This is illustrated schematically by the "block" structure drawn on the samples in Figs. 1 and 5. The block represents the extent of a region of the sample that scatters coherently; adjacent blocks have distinct phase differences between them. The argument given above may be generalized to say that any variations of the internal vertical structure of the blocks (such as d-spacing disorder) cannot be the origin of the phase difference, because such structure will always give rise to features that are very broad ($\sim 2\pi/t$) along the q_Z direction. To accrue a phase shift of the order of π between adjacent blocks, it is necessary to have a height difference between their outermost diffracting planes of half a superlattice period, of 19 Å, which seems to be reasonable over a lateral distance of 60 μm for the variation of film thicknesses out of a total of 15 000 Å grown. Since we estimated there were of order eight clear speckles in the pattern, we conclude there must be of order eight such distinct "blocks" within the footprint of the coherent beam.

Assuming this block model of the sample then allows us to construct a functional description of the speckle. We can assume the diffraction from each block to be perfectly specular, and to differ from that of its neighbor only by an arbitrary phase associated with the local height of the multilayer modulations above the substrate. When illuminated by a perfectly coherent x-ray beam the sample may be considered to be a *linear phase array* emitting wave fronts with a different phase from each block. If x represents the position across the beam, which extends over the range $0<x<d_1$, at the sample position, then the phase of the diffracted beam can be approximated by a discrete value corresponding to each of the N blocks,

$$\phi(x)=\phi_j,\quad (j-1)d_1/N<x<jd_1/N\ ,\quad j=1,\ldots,N\ .$$

If we observe the superposition of the wave fronts on a screen a large distance D from the sample, then we find the amplitude variation with position on the screen y is given by the standard Fraunhofer integral[10]

$$\begin{aligned}A(y)&=\int_0^{d_1}\exp\left[2\pi i\frac{xy}{\lambda D}\right]\exp[i\phi(x)]dx\\&=\sum_{j=1}^{N}\int_{(j-1)d_1/N}^{jd_1/N}\exp\left[2\pi i\frac{xy}{\lambda D}\right]\exp(i\phi_j)dx\\&=\sum_{j=1}^{N}\exp\left[2\pi i(j-\tfrac{1}{2})\frac{d_1y}{N\lambda D}\right]\exp(i\phi_j)\\&\times\int_{-d_1/2N}^{d_1/2N}\exp\left[2\pi i\frac{xy}{\lambda D}\right]dx\\&=\frac{\sin(\pi d_1y/N\lambda D)}{\pi y/\lambda D}\\&\times\sum_{j=1}^{N}\exp\left[2\pi i(j-\tfrac{1}{2})\frac{a_1y}{N\lambda D}+i\phi_j\right]\ .\end{aligned}\tag{1}$$

Thus the diffraction pattern is seen to be the product of a wide $\sin(x)/x$ slit function with a width corresponding to the *block* size, multiplied by a complex "random-phase sum" over the block phases ϕ_j. This random-phase sum modulates the amplitude within the envelope of the block slit function, thereby providing the two length scales seen in our speckle patterns: the width of the fine structure (individual speckles) arises from the size of the beam; the envelope width comes from the size of the coherently scattering blocks; the penetration depth and overall depth of the sample are too small to contribute.

The screen in the discussion above is, of course, the position of our back pinhole (see Fig. 1), or of a film or position-sensitive detector in other experiments. Thus the observed intensity through this second pinhole is just the square modulus of Eq. (1) convolved with a box function with the size of the pinhole. In our case the back pinhole was $d_2=20$ μm at a distance of $D=1.3$ m; this is sufficiently small that the convolution represents only a correction to the widths. The square modulus of Eq. (1) was therefore used to compare directly with the data.

V. FITTING PROCEDURE

We found it was necessary to devise a special fit procedure to avoid the dangers of multiple local minima inherent in fitting a function with as many free parameters as Eq. (1). While the dimensional parameters were known and the number of blocks, N, could reasonably be estimated as above, we have no *a priori* information about the phases ϕ_j. We therefore alternated cycles of least-squares refinement (Marquardt algorithm[11]) with cycles of χ^2 searches. Both systematic mesh searches and random (Monte Carlo) searches were employed. The searches were limited to just the phases, while the least-squares refinement was applied to the phases and five additional parameters: a constant background level, a background slope, a peak center position, a scale factor, and an overall peak width. The alternation was found to be useful because the five additional parameters coupled somewhat to the choice of best phases. The entire pro-

cedure was repeated a sufficient number of times that the same local solution was generated more than once. We could therefore be reasonably certain that we had exhausted all phase possibilities and obtained the global minimum of χ^2.

The discrete parameter N was also varied systematically, and lower χ^2 values (χ^2 around 30) were found for $N=8$ than for $N<8$ or $N=9$. As expected, the number of peaks in the central maximum (the number of speckles) was found to be approximately equal to N (the number of independent blocks). Equation (1) can be seen to be identically zero when $y=N\lambda D/d_1$ (or multiples thereof), when the wide slit function passes through its nodes. Since the width of each speckle peak is fixed by the inverse of the front pinhole size, d_1, the criterion for the best value of N was found to correspond to locating the nodes at suitable low points in the data.

Examples of fits obtained in this way are shown passing through both sets of data in Fig. 4. During searching, the phase values were restricted to the range $-\pi<\phi_j<\pi$. The main peak positions, heights, and widths are fitted fairly well, but some smaller features are missed (see below). One reason for this imperfection is the discrete nature of the model, assuming exactly N equal-area blocks. In an attempt to further improve the fits, the individual block sizes were then allowed to vary by using a more general expression than Eq. (1) with N *variable* width blocks. Predictably, the addition of $N-1$ additional parameters permitted a better fit, reducing χ^2 a further 30%. However, we did not pursue *ab initio* fitting with this generalized model exhaustively and only used it to improve existing results. The solutions were therefore nearby in parameter space, and generated the dashed curves in Fig. 4. It is important to emphasize that *both* sets of data in Fig. 4, corresponding to two different positions on the sample, are fitted by the *same* model with different parameter values.

The best-fitting phases structures are shown pictorially for uniform block width in Fig. 6(a) and variable block width in Fig. 6(b). The maximum total phase excursion of $\pm\pi$ corresponds to a total height variation in the positions of the diffracting planes of one superlattice period, or 38 Å, and is indicated by dashed boundaries in Fig. 6. It should be noted that this is an artificial limitation, as Eq. (1) is inherently insensitive to phase shifts of multiples of 2π. Since large phase jumps in the picture are equivalent to small jumps to values outside the $\pm\pi$ boundary, the pictures have been drawn in a way (not unique) that minimizes the number of big jumps, to yield the smoothest-looking phase structures, but ones which have an overall phase variation somewhat greater than 2π. Also, more than one solution for the phases were found occasionally to be indistinguishable by their χ^2 values; closer examination typically showed a simple relation between the solutions, such as a reversal or mirror image of the phase sequence. The phase outcomes in Fig. 6 also appear to have some internal structure that is different from random: three consecutive phases are almost identical for the first sample position. This tells us that a single large block could have replaced three of the uniform-sized blocks in the model, so a variable-block-size model might be a more effective use of parameters in the general case.

Closer examination of the fits in Fig. 4 points to a more serious inadequacy of this model. There is a factor-of-2 discrepancy between the fitted values of the peak widths, $\lambda D/d_1$ in Eq. (1), and the values expected from the geometry. The fits give values of 49 and 62 μm for the two sample positions, but something like 28 μm (1.05 Å$\times$1.3 m)/(7 μm) convolved with 20 μm] is expected. As noted above, the observed widths of the speckles in the data do indeed correspond to that observed for the Fraunhofer *central* maximum, so the problem must lie with the fit function.

The discrepancy can be resolved by close examination of the form of the function in Eq. (1). When all the phases are equal, Eq. (1) becomes the ideal 1D Fraunhofer diffraction curve, which is a simple slit function, $[\sin(x)/x]^2$, where $x=\pi d_1 y/\lambda D$; this has a central maximum with a node-to-node width in y of $2\lambda D/d_1$ and side fringes of width $\lambda D/d_1$. When the phases are al-

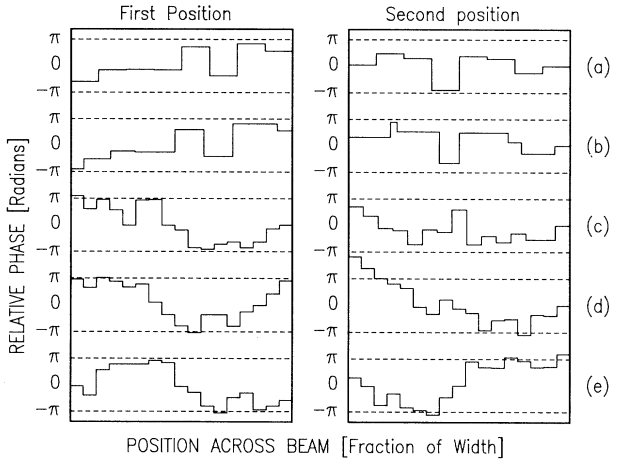

FIG. 6. Sketches of the linear N-phase structures which give the best-fit curves in Figs. 4 and 7 below. The ordinate is the relative phase of each block while the abscissa shows the spatial position of the blocks as fractions of the lateral dimension of the beam (extending over 500 μm of the sample). During refinement, the phase values were started in the range $-\pi<\phi<\pi$, but are indistinguishable from the values $\phi+2\pi n$. The phases have then been adjusted, modulo 2π, to take the value closest to their neighbors, but occasionally the choice is ambiguous. The phase of each block may be considered to be the relative height in the sample of the diffracting layers, on a scale where 2π corresponds to 38 Å (one superlattice period). Left and right panels represent the two positions measured on the sample. (a) The eight-phase fit to Fig. 4 (solid curve), using fixed block sizes. (b) The eight-phase fit to Fig. 4 (dashed curve), when the block sizes are then allowed to vary starting from the values in (a). (c) Best fits using the parameter search method with 17 phases (left) and 15 phases (right). These correspond to the dashed curve of Fig. 7 below. (d) and (e) Examples of fits with 17 phases using the "annealing" method. These correspond to the solid curves of Fig. 7.

lowed to vary, some side fringes become taller and the central one smaller until the identity of the original "center" is no longer distinct. The nodes become redistributed along the axis, so the node-to-node spacing becomes intermediate between $\lambda D/d_1$ and $2\lambda D/d_1$, with the taller peaks having greater widths than the smaller ones. When many peaks of equal size are caused to appear, their widths are closer to $\lambda D/d_1$ than $2\lambda D/d_1$. We fitted the data with $N=8$ phases because we identified about this number of speckles in the pattern. This assumed that every maximum in the fit function was a speckle peak, so the fitted value of the width was forced to enlarge to compensate.

If we now reassess the counting of speckles to admit that there are small peaks in amongst the big ones, the problem will be resolved. Close examination of the data shows there are indeed some small inflections between the major peaks as well as some shoulderlike features; these should all be counted as speckles as well. It may be more accurate to estimate the number of speckles as the number of nodes in the data rather than the number of big peaks. We therefore investigated fitting the data with $N\sim 16$ instead of $N=8$.

Unfortunately, with $N\sim 16$ the parameter is too large to handle by the parameter-search methods used before. In attempts to solve phase problems in crystallography, it is widely believed that to "guess" a structure, it is necessary to try at least four quadrature values for each phase degree of freedom.[12] The number of guesses for an N-phase structure is therefore 4^{N-1}. This is tolerable (16 000) when $N=8$ but unrealistically large (10^9) when N becomes 16. In spite of these tall odds, we attempted to fit the data by random parameter searching with a larger number of phases ($N=16$ or 17) and found satisfactory results after $\sim 2\times 10^5$ attempts. The best examples are shown in line (c) of Fig. 6, where the agreement with the data is substantially improved over Fig. 4. The dashed fit curves in Fig. 7 now have inflections between the large speckle peaks because smaller peaks have been introduced there, as expected. The resulting values of $\lambda D/d_1$ obtained by fitting, 32.7 and 37.4 μm, are now much more reasonable. Of course, we cannot claim these are global best fits because we did not sample enough starting phase combinations; they serve as examples of fits that are improved by using more phases, and which have resolved the discrepancy in the widths.

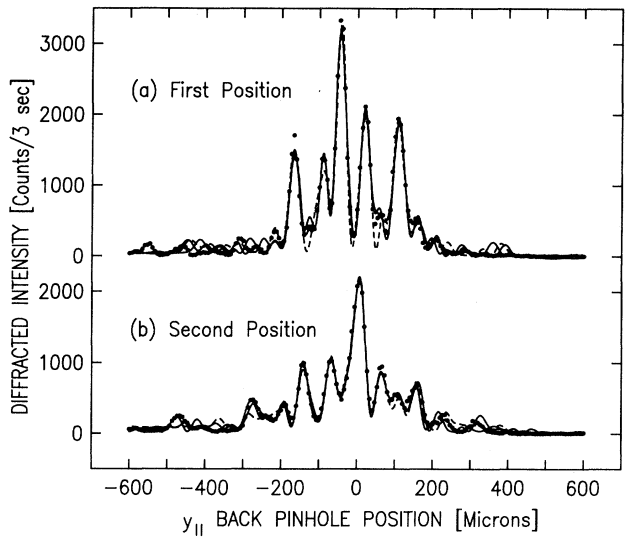

FIG. 7. Improved fits to the data of Fig. 4 using a greater number of phases. As no global best fit was obtained, several "good" examples are superimposed. All fits shown had a lower chisquare than the fits in Fig. 4. The dashed fit curve corresponds to structure (c) in Fig. 6, using the random-search method. The solid fit curves correspond to structures (d) and (e) in Fig. 6, using the "annealing" algorithm. (a) 17-phase examples with fitted $\lambda D/d$ widths of 35.0, 33.0, and 32.7 μm. (b) 17-phase and 15-phase examples with fitted $\lambda D/d$ widths of 39.9, 38.1, and 37.4 μm.

We tried one additional method for arriving at large-N phase solutions for these speckle patterns. Noting that the solutions even with $N=8$ tend to have groups of adjacent phases close to the same value, we might make an "educated" guess that, if an additional phase were added to an existing structure, it would be more likely equal to its neighbor's phase than opposite. This suggests a recursive method to extend a structure with N phases to one with $N+1$. If we start from an existing fit with N phases (on equal-sized blocks), we can compress the blocks into a new structure with N blocks each reduced in length by $N/(N+1)$, and add one new phase at the end with an initial value equal to its predecessor in the sequence. Because perturbations of the values of adjacent phases are correlated during least-squares refinement, the optimization by fitting this new structure with the data will accommodate the new phase and lead to a new best fit. We consider the least-squares fitting to be analogous to "annealing" the phase array after each addition of a new phase.

This "annealing" method was found to be much more effective than random searching for producing good fits to the data when we need large numbers of phases. Using one-tenth the total expenditure of computer time, half a dozen fits were found with better least-squares residuals. Two $N=17$ examples, each extended from $N=5$ starting structures, for each sample position are shown on lines (d) and (e) of Fig. 6, and as solid theory curves in Fig. 7. One again, the fitted width values are much more reasonable than for $N=8$, and agree roughly with the values expected from the geometry. The ultimate outcome was found to depend on the exact choice of starting structure, the constraints applied on the range of parameters, and the number of refinement cycles carried out at each phase addition. As before, it is not possible to say whether these fits are anywhere close to the global minimum, but the qualitative agreement with the data in Fig. 7 can certainly be claimed to be good.

It is clear that the various examples of fits in the different lines of Fig. 6, thought not identical, are closely related to each other. It should be remembered that left-right and up-down mirror images give identical fits, and the choice of which one is generated is arbitrary, due to the random factors involved in initiating the fit procedure. The structures are all characterized by regions of

roughly constant or slowly varying phase followed by sudden jumps. The jump positions are located faithfully in every fit. These must correspond to locations of growth defects in the multilayers, and may arise from instabilities such as step bunching during growth.[13]

VI. CONCLUSIONS

Several significant conclusions about the understanding of speckle patterns have arisen from this study. First, even when a symmetric beam is used, strongly anisotropic speckle can result from the use of a grazing geometry. Secondly, when the penetration depth is so much smaller than the lateral dimensions of the coherently diffracting domains, the vertical structure of the sample becomes unimportant, because its effects become smeared out by the finite-size broadening due to the limited penetration. The relevant phase of the domain is then determined only by the relative position of the diffracting planes at the surface. Thirdly, the fine details of the speckle patterns observed can be understood by a "random-phase model," and, finally, two practical methods of solving for the values of a limited set of phases have been demonstrated.

We do not believe this is necessarily a unique description of speckle, but instead a working model that embodies some of its important characteristics. It invites further testing of more powerful ways of gaining information about the microscopic arrangement of domains within a small region of a sample. For example, if two speckle patterns were recorded before and after a sample displacement by *less than* the size of the beam's footprint, they would be related in a way that might allow phasing of the peripheral material. A sequence of difference measurements might then allow a complete phase map to be generated experimentally.

We note in closing that the coherent-diffraction technique described here may have some utility in nondestructive roughness evaluation of semiconductor materials on an important length scale. The method may be thought of as an extension of the traditional (i.e., incoherent) diffuse-scattering method, which probes the same length scales, but would see only an average broad distribution instead of the highly modulated pattern of Fig. 4. The use of coherent x rays therefore allows higher-order moments of the roughness to be perceived in addition. In this sense, coherent diffraction combines characteristics of both scattering and imaging techniques. The typical distances probed are also accessible to optical interferometry, scanning probe microscopies [scanning tunneling microscopy (STM) and atomic force microscopy (AFM)] or scanning electron microscopy (SEM). The coherent-diffraction method differs from all of these others, however, in that it probes the lateral variation in height of a diffracting layer *inside the material,* which is not necessarily related to its surface. In the case of a semiconductor heterostructure device, for example, used as a quantum well, it is the roughness of the *interfaces* that determine the electron scattering, and hence mobility, and this is precisely the roughness to which the diffraction method is sensitive.

ACKNOWLEDGMENTS

We thank the staff of ESRF, particularly P. Feder and H. Gleyzolle, for valuable assistance and hospitality during execution of the experiment. We were greatly assisted in the setting up of the experiment by G. B. Stephenson, S. Brauer, S. G. J. Mochrie, and M. Sutton. I. K. R. and S. B. D. acknowledge support from the U.S. National Science Foundation under Grants No. DMR93-15691 and No. DMR92-17956.

[1]G. Grübel, J. Als-Nielsen, D. Abernathy, G. Vignaud, S. Brauer, G. B. Stephenson, S. G. J. Mochrie, M. Sutton, I. K. Robinson, R. Fleming, R. Pindak, S. Dierker, and J. F. Legrand, ESRF Newslett. **20**, 14 (1994).

[2]M. Sutton, S. G. J. Mochrie, T. Greytak, S. E. Nagler, L. E. Berman, G. A. Held, and G. B. Stephenson, Nature **352**, 608 (1991).

[3]Z. H. Cai, B. Lai, W. B. Yun, I. McNulty, K. G. Huang, and T. P. Russel, Phys. Rev. Lett. **73**, 82 (1994).

[4]S. Brauer, G. B. Stephenson, M. Sutton, R. Brüning, E. Dufresne, S. G. J. Mochrie, G. Gübel, J. Als-Nielsen, and D. L. Abernathy, Rev. Sci. Intrum. **66**, 1506 (1995).

[5]S. B. Dierker, R. Pindak, R. M. Fleming, I. K. Robinson, and L. Berman, Phys. Rev. Lett. **75**, 449 (1995).

[6]B. Chu, *Laser Light Scattering: Basic Principles and Practices* (Academic, San Diego, 1991).

[7]G. Grübel, J. Als-Nielsen, and A. K. Freund, J. Phys. (France) IV **4**, C9-27 (1994).

[8]J. Als-Nielsen, A. K. Freund, G. Grübel, J. Linderholm, M. Nielsen, M. Sanchez del Rio, and J. P. F. Sellschop, Rev. Sci. Instrum. **B94**, 306 (1995).

[9]J. W. Goodman, *Statistical Optics* (Wiley, New York, 1985).

[10]J. M. Cowley, *Diffraction Physics* (North-Holland, Amsterdam, 1975).

[11]W. H. Press, B. P. Flannery, S. A. Teukolsky, and W. T. Vetterling, *Numerical Recipes in C* (Cambridge University Press, Cambridge, England 1988).

[12]H. Lipson and W. Cochran, *The Determination of Crystal Structures* (Cornell University Press, Ithaca, 1966).

[13]M. D. Johnson, C. Orme, A. W. Hunt, D. Graff, J. Sudijono, L. M. Sander, and B. G. Orr, Phys. Rev. Lett. **72**, 116 (1994).